Experimental Study of Seismic Behaviors of As-Built and Carbon Fiber Reinforced Plastics Repaired Reinforced Concrete Bridge Columns

Shuenn-Yih Chang[1]; Yeou-Fong Li[2]; and Chin-Hsiung Loh[3]

Abstract: In order to reliably obtain seismic responses of as-built and repaired reinforced concrete bridge columns under near-fault ground motions, pseudodynamic testing of two bridge columns with a reduced scale of 2/5 was performed. Pseudodynamic test results reveal that a ductile member may have no chance to entirely develop its ductile behavior to dissipate seismic energy, because it may suddenly be destroyed by a significant pulse-like wave. The seismic performance of the two damaged bridge columns can be recovered after repair with carbon fiber reinforced plastics composite sheets. It is also experimentally confirmed that the flexural failure moment obtained from the pseudodynamic test is in good agreement with the plastic moment predicted by the ACI 318 code. As pseudodynamic test results are believed to be more accurate than numerical solutions, they can be considered as reference solutions in developing a finite-element model. An identical specimen was tested under cyclic loading to estimate basic properties of these columns, such as shear strength, flexural strength, and ductility, so that the seismic responses obtained from pseudodynamic tests can be thoroughly discussed. Furthermore, its hysteretic response may also be used to match a mathematical model to simulate the very complicated load-displacement relation for analysis.

DOI: 10.1061/(ASCE)1084-0702(2004)9:4(391)

CE Database subject headings: Cyclic tests; Pseudodynamic method; Seismic response; Rehabilitation; Bridges, concrete; Columns; Ground motion.

Introduction

On September 21, 1999, the Chi-Chi earthquake (Loh et al. 2000) struck the central region of Taiwan. The magnitude of this earthquake was measured to be $M_s = 7.6$ on the Richter scale, and there were 10 aftershocks whose magnitudes were greater than 6.0. In this area, there are many hundreds of bridges and approximately 10% of the bridge inventory experienced moderate-to-major damage. It seems that the use of old design codes, AASHTO 1969 and AASHTO 1971, is responsible for the severe damage, because a large number of the damaged or collapsed reinforced concrete bridges were designed based on these codes. The most significant examples of poorly designed bridge columns are the inadequate longitudinal bars due to cut-off at column mid-height and the widely spaced as well as poorly anchored transverse reinforcement. However, moderate-to-major damage was also observed in newly constructed bridges, which were designed according to new design codes (Taiwan Bridge Design Code 1995; AASHTO 1996). It seems that the cause of this damage is primarily due to the near-fault ground motion, which is characterized by a pulse-like motion that exposes the structural system to high seismic energy at the beginning of the ground acceleration record. To explore the capacity of reinforced concrete bridge columns, a series of cyclic loading tests were performed at the laboratory of the National Center for Research on Earthquake Engineering (NCREE) (Chang and Chang 1999; Hwang et al. 1999; Li and Chu 1999). These tests include two categories of columns. One category is for columns with substandard design details and the other is for those with well-designed details. In addition to these tests, this study will also aid the understanding of the seismic response of a reinforced concrete bridge column that is designed according to the updated version of the Taiwan Bridge Design Code (1995).

In nonlinear dynamic analysis, an idealized load-displacement model is generally required to determine the restoring force after the displacement is found. Thus, the accuracy of these numerical solutions is highly dependent upon the mathematical model, which is usually developed from a match with cyclic loading test results. As a result, to accurately obtain the seismic response of a reinforced concrete bridge column through a numerical procedure is a very difficult task, because the load-displacement model for a reinforced concrete bridge column is very complicated and consequently is hard to simulate accurately. This difficulty is because the hysteretic loop for a reinforced concrete bridge column generally displays stiffness and strength degradation and the pinching effect. Because the load-displacement relation is not used in the pseudodynamic testing method (Takanashi et al. 1975; Shing and Mahin 1983, 1984, 1987, 1990; Chang 1997, 2000, 2001, 2002a,b, 2003; Chang et al. 1998), it seems this technique can

[1]Assistant Professor, Dept. of Civil Engineering, National Taipei Univ. of Technology, No. 1, Section 3, Jungshiau East Rd., Daan Chiu, Taipei 106-08, Taiwan, Republic of China. E-mail: changsy@ntut.edu.tw

[2]Associate Professor, Dept. of Civil Engineering, National Taipei Univ. of Technology, Taipei 106, Taiwan, R.O.C.

[3]Professor, Dept. of Civil Engineering, National Taiwan Univ., Taipei 106, Taiwan, R.O.C.

Note. Discussion open until December 1, 2004. Separate discussions must be submitted for individual papers. To extend the closing date by one month, a written request must be filed with the ASCE Managing Editor. The manuscript for this paper was submitted for review and possible publication on November 1, 2001; approved on November 7, 2003. This paper is part of the ***Journal of Bridge Engineering***, Vol. 9, No. 4, July 1, 2004. ©ASCE, ISSN 1084-0702/2004/4-391–402/$18.00.

provide a more reliable solution when compared with the numerical solution.

The pseudodynamic testing method is basically the same as the step-by-step integration procedure for a time history analysis. At first, the test structure is idealized as a discrete system, then the equations of motion governing the dynamic behavior of the test structure are formulated. A step-by-step integration method is needed to solve the governing equations in performing a pseudodynamic test. It is worth noting that the inertial and damping properties in the equations of motion are, in general, analytically described (Shing and Mahin 1984) while the restoring forces are no longer expressed as the product of the displacements and stiffness matrix, as is usually seen in a step-by-step integration procedure. Rather, the restoring forces are experimentally measured in a pseudodynamic test. Hence, the difficulty in modeling accurately the load-displacement relations for inelastic structures disappears. This experimental measurement indicates that pseudodynamic tests will give more reliable test results than for the step-by-step time history analysis, because they do not involve any idealized mathematical model for the load-displacement relationship.

Even though a more accurate seismic response can be obtained from pseudodynamic tests, the application of this technique to investigate the seismic behavior of reinforced concrete bridge columns is very rare. In this study, three identical reinforced concrete bridge columns were fabricated. One column was used to perform the reversed cyclic loading test in order to obtain the basic properties of these specimens, and the other two were tested pseudodynamically so that accurate seismic responses and reliable hysteretic loops of the reinforced concrete bridge columns under near-fault ground motions can be achieved. In addition to pseudodynamic testing of the as-built bridge columns, the damaged bridge columns were repaired with carbon fiber reinforced plastics (CFRP) and retested pseudodynamically. This retesting is intended to determine whether the damaged reinforced concrete bridge column may be restored to an acceptable seismic performance after repair with CFRP composite sheets (Aschheim and Moehle 1992; Priestley et al. 1996; Reinhorn et al. 1998).

Fabrication of Specimens

Three identical reinforced concrete bridge columns with a scale of 2/5 were cast. The design of the specimens was based on the 1995 version of the Taiwan Bridge Design Code and is a standard design for the Taiwan Highway Bureau. The scaled-down bridge columns had a height of 3,250 mm and a rectangular cross section with a dimension of 750×600 mm. The longitudinal reinforcement consisted of 32 No. 6 (19 mm diameter) bars with a design yielding strength of $f_y = 420$ MPa, which were evenly distributed on all faces and throughout the height of the column with a constant concrete cover of 25 mm. The concrete had a design compressive strength of 21 MPa at 28 days. The transverse reinforcement was made up of No. 3 (10 mm diameter) stirrups with a design yielding strength of $f_y = 280$ MPa at a spacing of 100 mm. In addition, there are five confining crossties. The anchorage of the hoops and crossties at their two ends were 90 and 135°, respectively. Design details of the specimens are shown in Fig. 1. These design details result in a longitudinal reinforcement ratio of 1.95% and a transverse reinforcement ratio of 1.04%. It should be mentioned that the footing and the load stub were designed to exceed the capacity of the column.

The yield strengths of the longitudinal and transverse reinforcement were obtained by standard tensile tests on steel bar

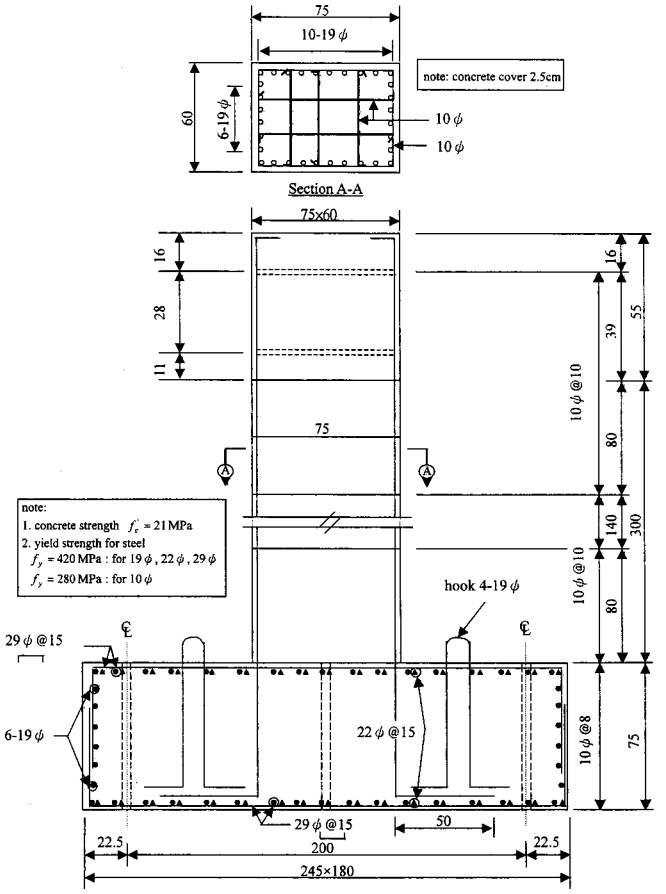

Fig. 1. Design details for reinforced concrete bridge columns

samples and were found to be 500 and 350 MPa, respectively. In addition, the concrete cylinders were tested to determine the concrete strength of the test specimens. The actual compressive strength of concrete was found to be 23 MPa at 28 days. In both cases, the actual strengths of the concrete and steel are higher than the design strengths.

Test Setup and Lateral Force Correction

The test setup for the cyclic loading test is implemented as shown in Fig. 2. In this setup, the test specimen was mounted on the strong floor and the reinforced concrete bridge column was axially loaded by a pair of 39 mm diameter high-strength pretension rods through a rigid beam that was placed across the top of the column. The lateral force was applied at the top of the specimen through a servo-hydraulic actuator, which was mounted horizontally on the reaction wall. The actuator was an MTS 243.70 single-ended static type. The built-in load cell and a linear variable displacement transducer (LVDT) were used to measure the restoring force developed by the specimen and the imposed displacement, respectively. Because the reinforced concrete bridge column will be simulated as a single degree of freedom (SDOF) system in performing the pseudodynamic test, the test setup is the same as that for the cyclic loading test.

In all of the tests, the axial load is taken to be 680 kN, which is often used by the Taiwan Highway Bureau to simulate a two-lane bridge deck. It should be mentioned that the axial load varies with lateral deflection, because the pretension rods necessarily

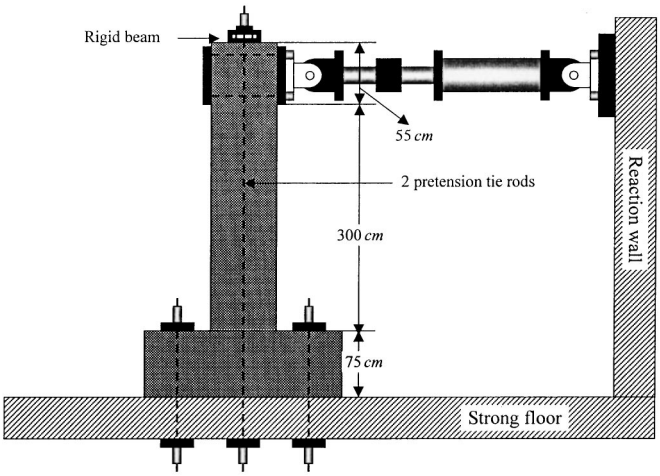

Fig. 2. Test setup for testing of reinforced concrete bridge columns

elongate when the bridge column deflects. A load cell is mounted on one end of each pretension rod and is used to measure the actual tension force for each rod. The symbol H represents the height of the bridge column and is equal to 3,250 mm while the depth of the footing plus the depth of the strong floor is denoted by h and is equal to 1,950 mm. Because the axial load of the reinforced concrete bridge column is vertically loaded through a pair of pretension rods during the test, it will not introduce any horizontal component force if the bridge column is undeformed. However, a horizontal component of the axial load is found if the bridge column is deformed horizontally. It is apparent that this horizontal component force will be included in the reading from the built-in load cell of the servo-hydraulic actuator. Hence, a correction of this measured force is necessary in order to realistically obtain the actual developed restoring force in performing either a cyclic loading test or a pseudodynamic test.

The details of the lateral force correction are schematically shown in Fig. 3. In this figure, the centerline of the bridge column coincides with the centerline of the pretension rods when the horizontal displacement is zero at the point where the servo-hydraulic actuator is imposed. However, when this horizontal displacement is nonzero, the centerlines no longer coincide, because the bridge column deforms like a cantilever beam while the pretension rod is deformed like a two-force member. The horizontal displacement for the centerline of the bridge column at the point where the servo-hydraulic actuator imposed is designated as d, and similarly the horizontal displacement for the centerline of the pretension rods is designated as $\bar{d}$. It is worth noting that the difference between d and $\bar{d}$ is very small, as their locations are close together at the top level of the bridge column. The imposed horizontal displacement will cause the pair of pretension rods to introduce a horizontal component force, and its value is equal to

$$P_h = P\bar{d}/\sqrt{d^2+(H+h)^2} \tag{1}$$

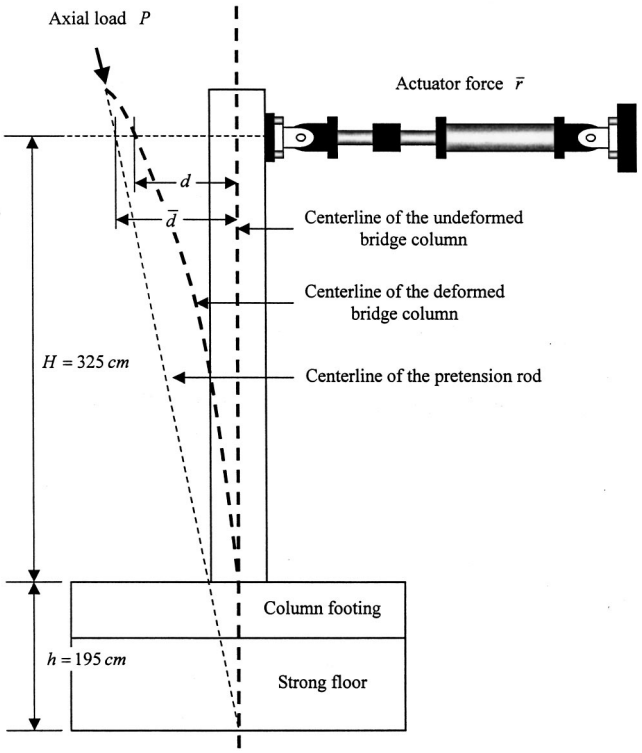

Fig. 3. Correction of lateral force

Because the value of d can be measured by the built-in LVDT within the servo-hydraulic actuator, $\bar{d}$ is not measured in the tests, and as $d \approx \bar{d}$, the displacement $\bar{d}$ was assumed equal to d in the computation of the horizontal component of the axial load. As a result, the restoring force actually developed by the test structure can be calculated by

$$r = \bar{r} - \frac{Pd}{\sqrt{d^2+(H+h)^2}} \tag{2}$$

where $\bar{r}$ = force from the load cell of the servo-hydraulic actuator; and P = measured axial load applied by the pair of pretension rods.

Cyclic Loading Test

A reversed cyclic loading test was conducted for Specimen A. The test was conducted in a displacement control mode, and the loading sequences of the column are shown in Table 1. In this table, the drift ratio is determined from the ratio of the imposed displacement over the height of the bridge column, H. Two displacement cycles were performed for each drift ratio.

Flexural cracks, perpendicular to the vertical column axis, initially occurred in the bottom region of the column at a drift ratio

Table 1. Loading Sequences for Cyclic Loading Test

	Cycle number									
Parameter	1, 2	3, 4	5, 6	7, 8	9, 10	11, 12	13, 14	15, 16	17, 18	19, 20
Drift ratio (%)	0.25	0.50	0.75	1.00	1.50	2.00	3.00	4.00	5.00	6.00
Displacement (mm)	8.125	16.25	24.38	32.50	48.75	65.00	97.50	130.0	162.5	195.0

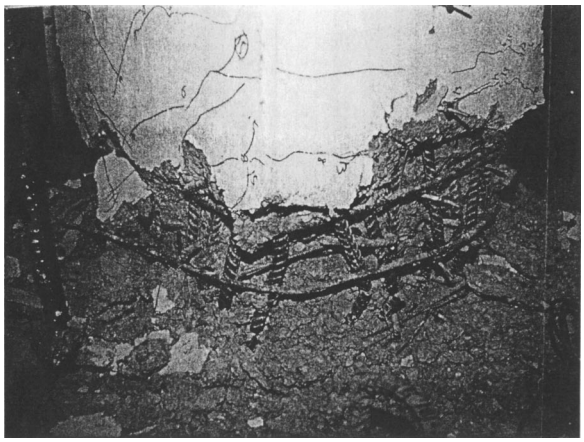

Fig. 4. Specimen A after cyclic loading test

of 0.25%. During the drift ratio of 1.5%, these cracks started to open. At the 3% drift ratio, they were widely opened and slightly spalled. Buckling of the longitudinal steel bars was visible at the drift ratio of 4%, while fracturing of the bars began at the drift ratio of 5%. A plastic hinge was formed near the bottom of the column during the test. However, there was no significant diagonal shear crack on the specimen at the end of the test. Thus, it is apparent that the failure mode of this specimen should be classified as a flexural failure. For this column, the crushing of concrete and the rupture of longitudinal steel bars at the end of the cyclic loading test can be seen in Fig. 4. The hysteretic response for Specimen A is shown in Fig. 5. In this figure, the load-displacement relation can be roughly considered to be linear when the drift ratio is smaller than or equal to 1.0%. The strength degradation between successive cycles became significant for drift ratios of 1.5% and larger. The rupture of a longitudinal steel bar can also be identified from the hysteretic loops where a sudden drop in the load is observed. The stiffness degradation can be seen in the hysteretic loops for the different drift ratios.

Pinching of the hysteretic loops was also explicitly observed for large drift ratios, although the specimen is a well-designed reinforced concrete bridge column. Pinching is characterized by the negligible stifness of the specimen as it passes through zero displacement, which leads to less energy dissipation per cycle when compared to a hysteretic loop without pinching. Pinching

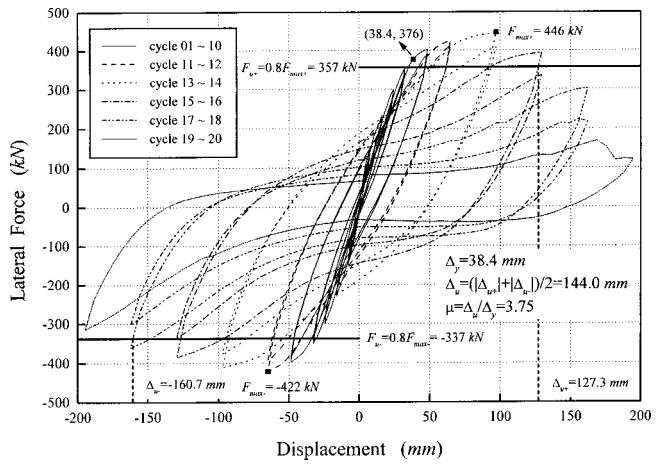

Fig. 5. Hysteretic response for Specimen A

might arise from the slippage of the longitudinal bars and the closing of flexural cracks in the plastic hinge zone of the reinforced concrete bridge columns. Because of the test setup, the axial load varied with lateral deflection. An average value of the axial load for the complete test is found to be 716 kN and a maximum value of 916 kN was found at a lateral displacement of 195 mm. Because this average value is slightly larger than (about 5%) the expected value of 680 kN, a slight increase in shear and moment capacities is anticipated. However, this increase must be very small. On the other hand, the $P-\Delta$ effect will be increased by the slight increase in axial load as a large lateral displacement is imposed. Apparently, the extra $P-\Delta$ effect due to the increase in axial load is not very significant, because the increase in axial load is only about 5% and the maximum lateral displacement is 195 mm in the test.

The yield displacement of the specimen, accounting for second-order effects, is estimated using the analytically calculated yield moment, $M_y=1{,}248$ kN-m, and the experimentally obtained hysteretic loop shown in Fig. 5. The yield displacement was found to be 38.4 mm at an applied lateral force of $F=376$ kN. This data point is indicated by a solid square symbol in Fig. 5. This yield displacement of $\Delta_y=38.4$ mm is used to determine the displacement ductility herein. Meanwhile, the ultimate lateral force of the specimen is defined as being 80% of the maximum lateral force from testing, and the corresponding displacement is considered as the ultimate lateral displacement (Priestley et al. 1996). Applying these definitions, maximum lateral forces, ultimate lateral forces, and ultimate lateral displacements in both push and pull directions are shown in Fig. 5, where the subscript "+" represents the push direction and the pull direction is denoted by the subscript "−". As a result, the average value of the maximum lateral forces, the ultimate lateral forces, and the ultimate lateral displacements are $F_{\max}=434$ kN, $F_u=347$ kN, and $\Delta_u=144.0$ mm, respectively. Hence, the ductility for the specimen is $\mu=\Delta_u/\Delta_y=3.75$. Finally, the ultimate flexural moment is estimated to be $M_u=F_uH+P\times\Delta_u=1{,}226$ kN-m.

On the other hand, according to the provisions of ACI 318, and using the actual strength of steel and concrete, the nominal flexural strength of the reinforced concrete bridge column is computed to be $M_n=1{,}480$ kN-m and the plastic moment capacity is $M_p=1.25\,M_n=1{,}850$ kN-m. Employing the equation developed by Aschheim and Moehle (1992), the nominal shear strength is found to be $V_n=750$ kN. As a result, the design shear strength is $V_d=\phi V_n=638$ kN, where the shear strength reduction factor ϕ is 0.85. These computation results attest to a flexural failure of the specimen, because the ultimate lateral force from testing, $F_u=347$ kN, is far less than the design shear strength $V_d=638$ kN and the ultimate flexural moment $M_u=1{,}226$ kN-m is close to the design flexural strength $M_d=\phi M_n=1{,}140$ kN-m, where ϕ=strength reduction factor and is computed to be 0.77 for this case.

In the Taiwan Bridge Design Code (Taiwan 1995), the total cross-sectional area of transverse reinforcement for a rectangular reinforced concrete column shall not be less than the greater value of the following equations:

$$A_{sh}=0.30ah_c\frac{f'_c}{f_{yh}}\left(\frac{A_g}{A_c}-1\right)$$
$$A_{sh}=0.12ah_c\frac{f'_c}{f_{yh}}\left(0.5+1.25\frac{P_e}{f'_cA_g}\right) \quad (3)$$

where a=vertical spacing of hoops (stirrups) in mm with a maxi-

mum of 150 mm; A_c=area of the concrete core in mm^2 measured to be the outside of the transverse reinforcement; A_g=gross area of column in mm^2; A_{sh}=total cross-sectional area in mm^2 of hoop (stirrup) reinforcement including supplementary cross ties (note that this should be calculated for both principal axes of a rectangular column); f'_c=specified compressive strength of concrete in MPa; f_{yh}=yield strength of hoop or spiral reinforcement in MPa; h_c=core dimension of tied column in mm; and P_e=factored load in kN.

These design equations and other design requirements for transverse reinforcement for confinement at plastic hinges are the same as those specified in AASHTO (1996) for seismic performance categories C and D, except that a maximum vertical spacing of 100 mm is adopted and the second line of Eq. (3) is replaced by $A_{sh}=0.12ah_c(f'_c/f_{yh})$ in AASHTO (1996). It is found that the transverse reinforcement used in the tested columns for confinement is insufficient to meet the requirement of $A_{sh}=0.12ah_c(f'_c/f_{yh})$. This requirement implies that a better ductility may be achieved if using the design details of AASHTO (1996) for reinforced concrete for seismic performance categories C and D.

Pseudodynamic Test Procedure

A structure has to be idealized as a discrete-parameter model in order to be tested pseudodynamically. In addition, the reliability of pseudodynamic test results essentially depends on the realism of the idealized test model. In general, the dead load of the reinforced concrete bridge column originates from the weight of the cap beam, the girders, and the deck. Therefore, it is appropriate to analytically simplify the bridge column as a single degree of freedom (SDOF) system where the lateral displacement at the top level of the bridge column is taken as the only degree of freedom. As a result, the total mass attributed to the bridge column is lumped at this degree of freedom. The equation of motion for this SDOF system is found to be

$$m\ddot{u}+c\dot{u}+ku=f \tag{4}$$

where m, c, and k are used to denote the mass, viscous damping, and stiffness; u, $\dot{u}$, and $\ddot{u}$ represent the nodal displacement, velocity, and acceleration at the point where the servo-hydraulic actuator is imposed, respectively; and f is used to represent the external nodal force. It should be mentioned that the term ku is generally replaced with the restoring force r in performing a pseudodynamic test, because the stiffness is very hard to determine accurately during the test.

Many step-by-step integration algorithms can be employed to solve the equation of motion. The Newmark explicit method (Newmark 1959), where acceleration is assumed to be constant within each time step, is used in this study; its general formulation is

$$\begin{aligned} &ma_{i+1}+cv_{i+1}+r_{i+1}=f_{i+1} \\ &d_{i+1}=d_i+(\Delta t)v_i+\frac{1}{2}(\Delta t)^2a_i \\ &v_{i+1}=v_i+\frac{1}{2}(\Delta t)(a_i+a_{i+1}) \end{aligned} \tag{5}$$

where d_{i+1}, v_{i+1}, and a_{i+1}=approximations to the displacement, velocity, and acceleration at the $(i+1)$th time step. In addition, r_{i+1} is introduced to denote the restoring force actually developed by the test specimen at the end of $(i+1)$th time step. Damping is difficult to model, because various damping mechanisms may exist in a structure, such as Coulomb damping, viscous damping, and hysteretic damping. Hysteretic damping and Coulomb damping are automatically taken into account in a pseudodynamic test procedure, while viscous damping is specified in the equation of motion. Because of the difficulty in separating one damping effect from the other in a pseudodynamic test, it is almost impossible to determine the exact viscous damping property of the test specimen. Even though viscous damping is included in Eqs. (4) and (5) for completeness, it will be assumed to be zero in this study. This assumption is justified because the hysteretic damping is the major source of damping to dissipate seismic energy for the reinforced concrete bridge column and will be automatically taken into account in the pseudodynamic test.

The following execution steps are a summary of using the Newmark explicit method to perform the pseudodynamic tests starting at the beginning of the $(i+1)$th time step:

1. Calculate the displacement d_{i+1} for this time step by using the second line of Eq. (5).
2. Impose the computed displacement d_{i+1} upon the test specimen by using the servo-hydraulic actuator.
3. Immediately read the force $\overline{r_{i+1}}$ from the built-in load cell right after the stop movement of the actuator, then use Eq. (2) to calculate the actual restoring force r_{i-1} developed by the test structure.
4. Compute the acceleration a_{i+1} and the velocity v_{i+1}.
5. Repeat steps 1–4.

This pseudodynamic test procedure can be repeated until the desired response time history is achieved.

Pseudodynamic Results for As-Built Specimens

It is believed that many buildings and bridges were damaged or even collapsed due to the strong near-fault ground shaking during the Chi-Chi earthquake (Loh et al. 2000). Therefore, it is interesting to pseudodynamically evaluate the seismic performance of reinforced concrete bridge columns under this type of ground motion. Many near-fault ground motion data were collected by the Central Weather Bureau under the Taiwan Strong Motion Instrumentation Program during the main shock of Chi-Chi earthquake, which was caused by the rupture of the Chelungpu Fault. The ground accelerations recorded from stations TCU075 and TCU102 during this earthquake are chosen as the seismic input in this investigation. The ground acceleration and the ground velocity for TCU075 and TCU102 are plotted in Figs. 6 and 7, respectively, where the velocity-wave form is computed from the ground acceleration data through a baseline correction and integration process. It can be seen from the two bottom plots that a pulse-like wave in the velocity-wave form is identified for TCU075 and TCU102. This pulse-like wave may have significant influence on the seismic response of a structure, because it will impose high seismic energy on the structure.

A reinforced concrete bridge column is simulated as an SDOF system with a concentrated mass at the top of the bridge column. The lumped mass for Specimen B is assumed to be 27,500 kg and the system is subjected to the ground acceleration record of TCU075 with a peak ground acceleration of 0.8g. Meanwhile, the lumped mass for Specimen C is specified to be 68,000 kg and the system is excited by TCU102 with a peak ground acceleration of 0.7g. It was estimated by the IDARC program that the peak ground acceleration of 0.8g for TCU075 and that of 0.7g for TCU102 are the maximum earthquake inputs that will not col-

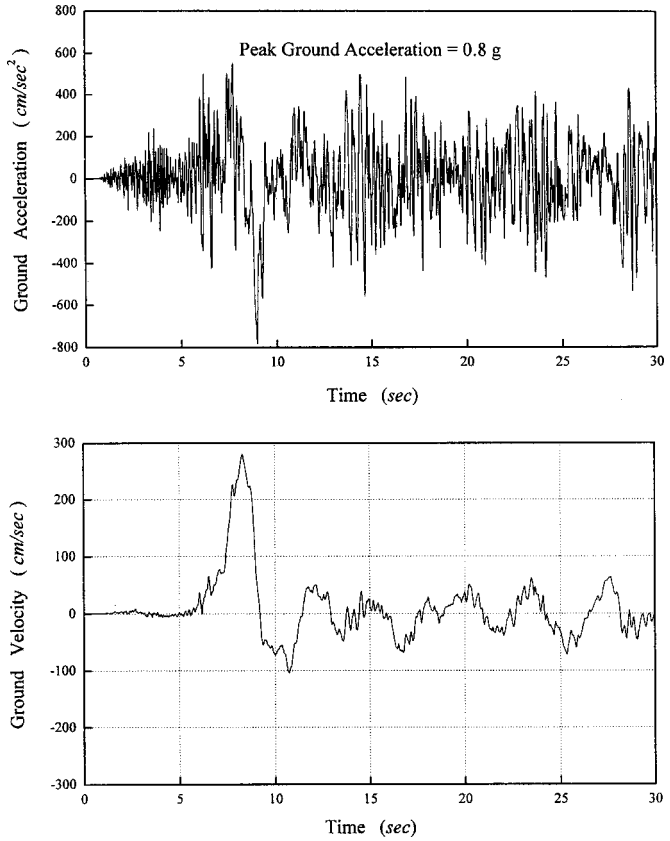

Fig. 6. Ground acceleration and velocity for TCU075

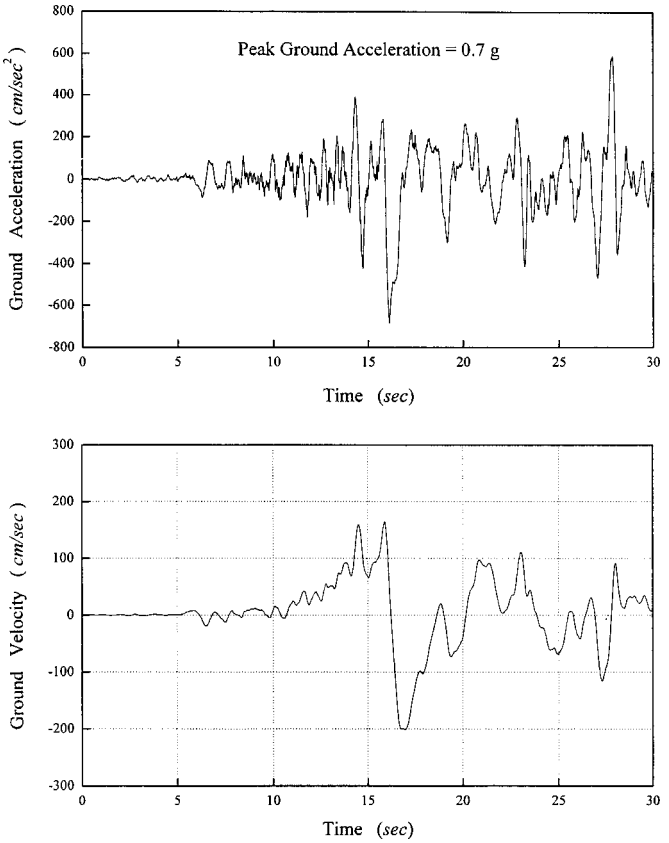

Fig. 7. Ground acceleration and velocity for TCU102

lapse the specimens. Both pinching and softening effects for a reinforced concrete bridge column have been considered in the IDARC program (Reinhorn et al. 1998). In fact, strength softening is used to define the reduction in component strength capacity under cyclic loading after reaching the ultimate strength limit. Pinching is used to define the ratio of the retained stiffness to the initial stiffness on the unloading path.

The rate of loading imposed upon the specimen was taken to be 0.1 mm/s in performing all the pseudodynamic tests. Pseudodynamic test results for Specimens B and C are plotted in Figs. 8 and 9, respectively. Each figure consists of two plots. The top plot shows the time history of the displacement response, and the hysteretic response is depicted in the bottom plot. In Fig. 8, it can be seen that maximum values of the displacement and lateral force were reached at a time of $t=14.52$ s and were 68.3 mm and 467 kN, respectively. The maximum flexural moment also occurred at this time and was found to be 1,563 kN-m, which is less than the plastic moment capacity $M_p=1{,}850$ kN-m. The maximum ductility experienced is found to be $\mu_{\max}=\Delta_{\max}/\Delta_y=1.78$ at this time, where $\Delta_{\max}=68.3$ mm and $\Delta_y=38.4$ mm. Stiffness degradation can be seen in the hysteretic response. It seems the reinforced concrete bridge column can effectively dissipate the seismic energy through ductile behavior. At the end of this test, yielding of some longitudinal steel bars was detected, but there was no buckling among them. However, flexural cracks were found and slight spalling of concrete cover was also observed, as can be seen in Fig. 10. In general, this column was not damaged to a point of loss, because the maximum lateral force and the maximum flexural moment are less than the shear capacity and the plastic moment capacity, respectively. Furthermore, the maximum ductility experienced is less than the ductility ratio of 3.75 determined from the cyclic loading test.

In the top plot of Fig. 9, it can be seen that the pseudodynamic test was stopped at $t=16.25$ s because the concrete cover was severely spalled, some longitudinal steel bars were buckled, and some of these were almost fractured at the bottom of the bridge column. At this time, the horizontal displacement at the top of the bridge column was as large as 250 mm, which corresponds to a drift ratio of 7.7%. However, in order to clearly display the time history and hysteretic loops for the two plots shown in the figure, the lateral displacement was plotted in the range of ± 150 mm, not ± 250 mm. Very significant stiffness degradation and a very large amount of energy dissipation were observed during the time interval of $14 \leqslant t \leqslant 15$ s. It is clear that the reinforced concrete bridge column cannot survive the significant pulse-like wave, which has a peak ground velocity at the time of $t=16.78$ s, as shown in Fig. 7. A drastic softening of the bridge column was found as the very significant pulse-like wave struck it. These hysteretic loops reveal that a well-designed reinforced concrete bridge column might have no chance to develop its energy dissipation capacity when subject to the very intense ground shaking of the near-fault ground motion. In fact, the near-fault ground motion usually contains pulse-like velocity wave forms that may be more destructive than the peak ground acceleration for some structures. Meanwhile, it can be found that the maximum lateral force is as large as 551 kN at $\Delta_u=144.0$ mm, which is the ultimate lateral displacement defined previously and is larger than that for Specimen A. This result might be due to the fewer cycles of loading when compared with those of Specimen A. In addition, the flexural failure moment of this bridge column is found to be 1,870 kN-m and is almost exactly predicted by the ACI 318 code with the value of $M_p=1{,}850$ kN-m. As a result, a flexural failure mode can be identified, and this result seems to experimentally

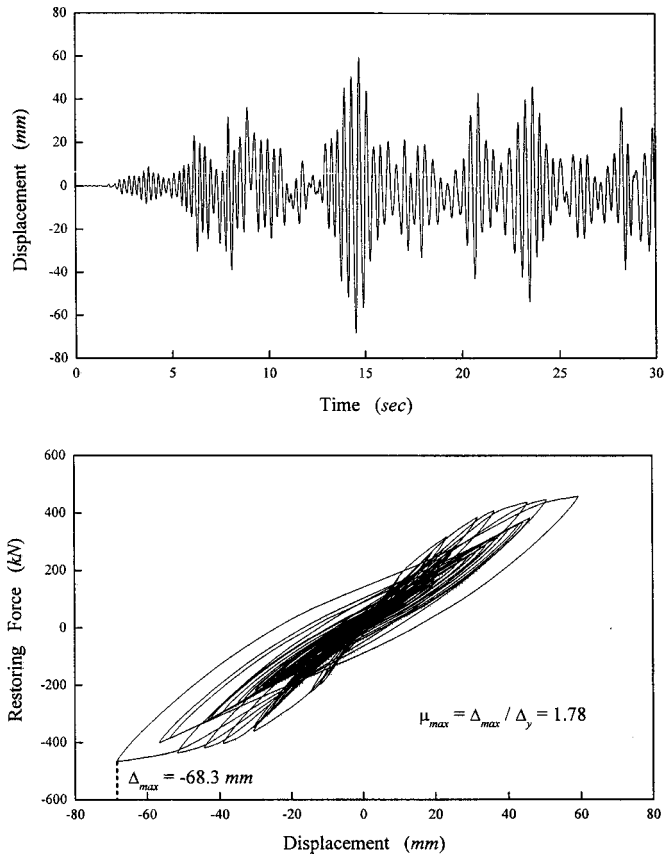

Fig. 8. Pseudodynamic results for as-built Specimen B subject to TCU075 with PGA=0.8*g*

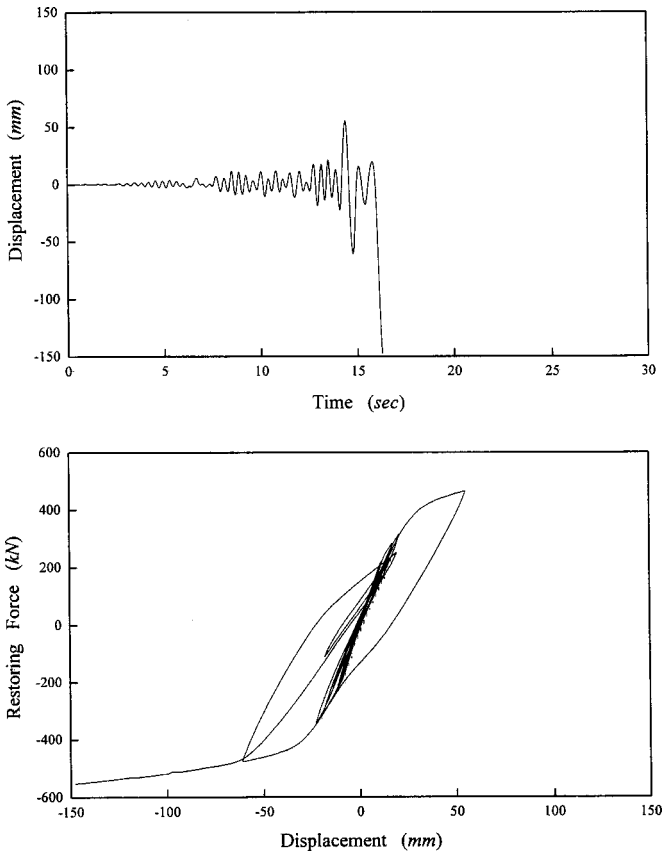

Fig. 9. Pseudodynamic results for as-built Specimen C subject to TCU102 with PGA=0.7*g*

confirm that the plastic moment estimated by the ACI 318 code is very reliable. The maximum displacement ductility observed in this specimen was approximately 6.5 when the test was stopped and was 3.75 at the maximum applied load. This indicates, despite the extreme loading associated with the pulse, that good ductility was achieved, exceeding that observed in the cyclic test.

Repair of Damaged Specimens with Carbon Fiber Reinforced Plastics Composite Sheets

Some bridges that were designed to modern codes were also damaged or even failed during the Chi-Chi earthquake. This damage may be because: (1) the fault rupture was directly under or between bridge foundations; or (2) near-fault ground motions are very intense and extremely punishing to these bridges. It was urgent to restore the damaged bridges immediately following the catastrophic earthquake due to the need to reopen highways for emergency rescue. Because CFRP reinforcement possesses excellent properties, such as low weight, high strength, and high corrosion resistance, and because it is much easier to handle on site, this material was widely chosen for repairing and retrofitting immediately after the Chi-Chi earthquake.

It is very interesting to study the seismic performance of the damaged reinforced concrete bridge columns after repair with CFRP composite sheets. Because the test specimens for this study were designed to the new code, there was no specific structural deficiency, such as shear strength, flexural strength, and ductility, based on the new design code. Damage to the specimens originates from the very intense near-fault ground shaking, which is much larger than the design earthquake load. Thus, repair is intended to restore the design strength to the preseismic event capacity. Both columns were wrapped with CFRP composite sheets, which were manufactured by the Industrial Technology Research Institute in Taiwan. The fibers within the CFRP composite are unidirectional. Mechanical properties of the component carbon fiber are summarized in Table 2. Properties of the CFRP wrap will be lower than these.

Because Specimens B and C were damaged and failed in the plastic hinge zone, the repair of these specimens was focused in this area. Since reinforcing bar fractures occurred in Specimen A,

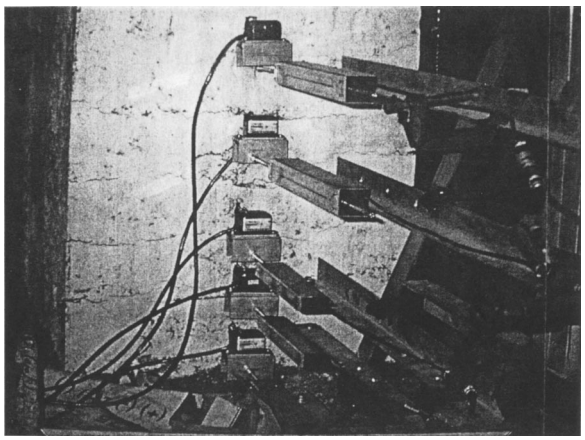

Fig. 10. As-built Specimen B after pseudodynamic test

Table 2. Properties of Carbon Fiber Reinforced Plastics (CFRP)

Property	CFRP
Thickness of layer (mm)	0.1375
Width of layer (mm)	400
Component fiber ultimate strength (MPa)	4,200
Component fiber elastic modulus (MPa)	235,000
Component fiber ultimate strain (%)	1.8

this specimen could not be repaired with CFRP sheets alone and was not retested. At first, the damaged concrete cover was removed and replaced with nonshrink mortar. It is worth noting that there was no treatment for steel bars, because they did not break. However, the tilted specimen was moved back to its original position by using the servo-hydraulic actuator before repair, although this might not be feasible in the field. It is worthwhile to note that the as-built Specimen C under TCU102 with a peak ground acceleration of 0.7*g* will collapse in practice, because the test was stopped at a specified maximum displacement of 250 mm although the time step was not completed in the pseudodynamic test. This emergency stop was intended to protect the specimen from collapse so that it could be repaired and retested. Thus, this specimen is more likely to be demolished than repaired in practice. Next, all the corners of the test specimens were beveled and rounded to a radius of 30 mm to reduce stress concentrations in the CFRP composite sheets that occur due to the rectangular geometry of the cross section. The calculation of repair thickness for the CFRP composite sheet at the potential plastic hinge zone is based on force-based design (Caltrans 1986) and the resulting required thickness is 0.31 mm. Thus, three layers of the CFRP composite sheets, whose total thickness is 0.41 mm, were applied in the potential plastic hinge zone, which was about 1/4 of the column height, i.e., in the 800-mm-long portion of the bridge column above the top of the footing. Meanwhile, a single layer was wrapped around the rest of the column, although there is no need to repair this portion of the column. The CFRP composite sheets wrapped around the bridge columns in this manner are intended to provide external confinement, to prevent spalling and crushing of the concrete cover, and in turn to prevent buckling of the longitudinal reinforcement.

Pseudodynamic Results for Repaired Specimens

Tests for the repaired Specimens B and C were performed in the same manner as the as-built Specimens B and C. Results for the repaired Specimen B are plotted in Fig. 11, while those for the repaired Specimen C are depicted in Fig. 12. The results for the as-built column are also superimposed in Fig. 11 for Specimen B and in Fig. 12 for Specimen C so that the differences in seismic responses between the as-built and repaired columns can be easily observed.

For comparison, the initial stiffness for each pseudodynamic test specimen was determined from the first 3 s of each displacement response time history through a linear curve fitting method and is listed in Table 3, where K_0 denotes the initial stiffness and f_0 is used to represent its corresponding structural frequency. This table clearly shows that the initial stiffness after repair is only about 72% of that of the as-built bridge column for Specimen B while that for Specimen C is only about 74%. The reduced stiffness of the repaired specimens can likely be accounted for by the fact that the CFRP jacket is not bridging the crack at the column/

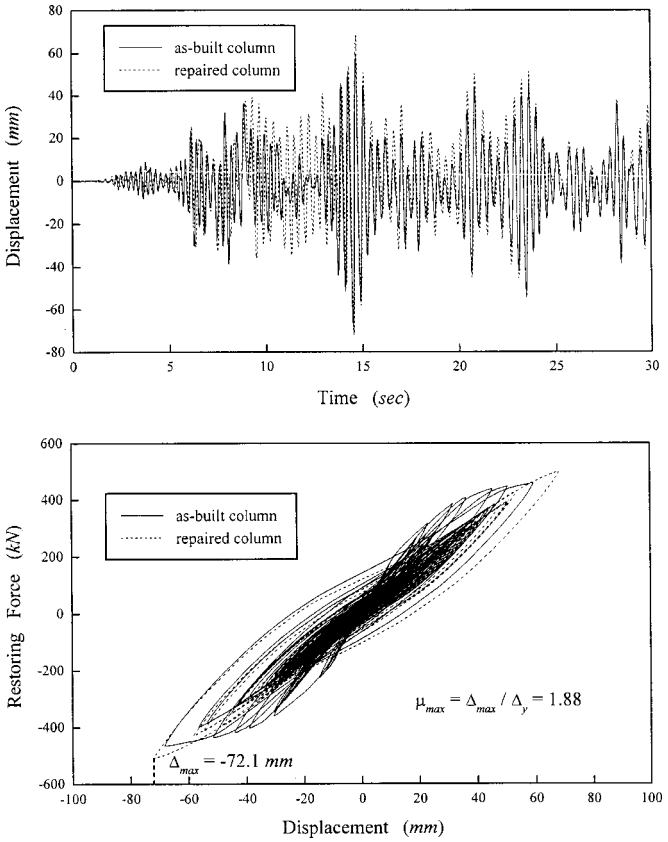

Fig. 11. Pseudodynamic results for repaired Specimen B subject to TCU075 with PGA=0.8*g*

footing interface. Additionally, any yielding of the longitudinal steel may have penetrated the footing and will result in a reduced lateral stiffness of the column. However, the strength and ductility of the repaired bridge column may be largely restored after the CFRP composite sheets are engaged and external confinement is developed at larger lateral displacements.

In Fig. 11, it can be seen that the displacement response time history of the same column before and after repair is very similar except that a slightly larger displacement response occurs during testing of the repaired specimen. In fact, the maximum displacement and maximum lateral force which occurred at the time of $t=14.55$ s were found to be 72.1 mm and 510 kN, respectively, and the maximum flexural moment was 1,705 kN-m. In addition, the maximum ductility is found to be 1.88, as shown in the bottom plot of this figure. Thus, it seems that the seismic performance of the damaged Specimen B was recovered after repair with CFRP composite sheets. The hysteretic loops shown in Fig. 11 reveal that the flexural stiffness of the repaired Specimen B is relatively more stable than that of the as-built Specimen B. The stiffness degradation is insignificant for the repaired Specimen B, while it can be observed for the as-built Specimen B. It is also very interesting to find from Fig. 11 that the lateral stiffness increases slightly, as the absolute value of the lateral displacement is greater than 20 mm. This result may be caused by the significant development of the hoop strain and corresponding concrete confinement in the CFRP composite sheets for a relatively large lateral displacement. At the end of the test, there were no observable flexural cracks on the outside carbon fiber layer along the fiber direction and no tension failure of the CFRP composite sheet.

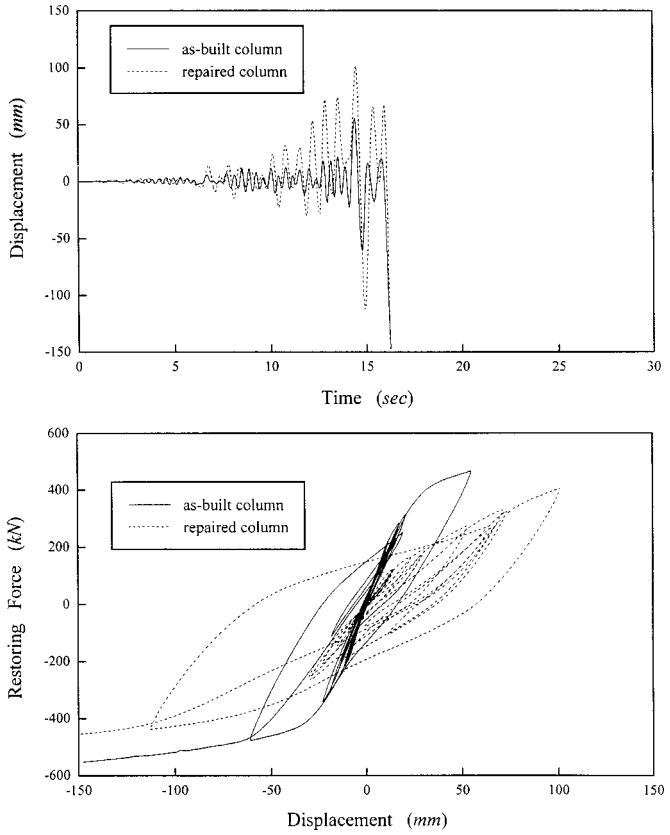

Fig. 12. Pseudodynamic results for repaired Specimen C subject to TCU102 with PGA=0.7 g

In Fig. 12, it is evident that the pseudodynamic test was stopped at $t=16.31$ s, since the outside carbon fiber layer had flexural cracks along the fiber direction and visible tensile failure of the CFRP composite sheet was also observed; both can be seen in Fig. 13. Furthermore, the CFRP composite sheets delaminated at the bottom of the column where bulging of the concrete was also observed. This condition also can be clearly seen in Fig. 13. Strain gauges measured the peak value of the hoop strain in the CFRP at a location 75 mm above the top face of the footing to be 0.28%. At this time, the horizontal displacement at the top of the column was larger than 250 mm. It is found that the maximum lateral force is as large as 475 kN at $\Delta_u=144.0$ mm, which is the ultimate lateral displacement defined previously, and is larger than that for Specimen A. Similar to the as-built Specimen C, the maximum displacement ductility observed in this specimen was about 6.5 when the test was stopped and was 3.75 at the maximum applied load. Again, good ductility was achieved, exceeding that observed in the cyclic test. It is shown in the top plot of Fig. 12 that the displacement response is, in general, much larger than that of the as-built Specimen C. Furthermore, the stiffness and strength are considerably reduced when compared to the as-built

Table 3. Comparison of Initial Structural Properties

	As-built specimen		Repaired specimen	
Initial property	K_0 (kN/cm)	f_0 (Hz)	K_0 (kN/cm)	f_0 (Hz)
Specimen B	278.0	5.06	201.1	4.30
Specimen C	293.2	3.30	217.3	2.85

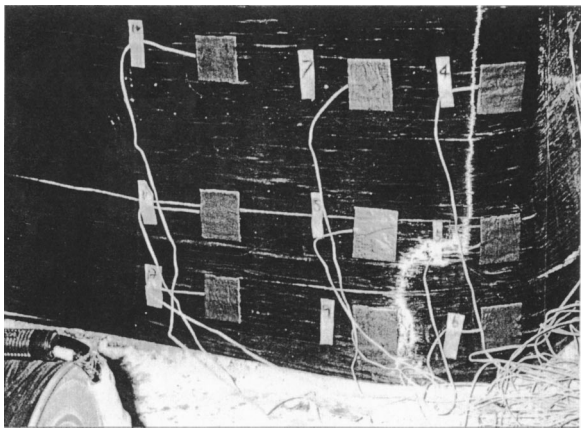

Fig. 13. Repaired Specimen C after pseudodynamic test

column as shown in the bottom plot of Fig. 12. The maximum lateral force was found to be 532 kN at the lateral displacement of 245 mm and the flexural moment at this time was 1,892 kN, which is very close to the flexural failure moment 1,870 kN for the as-built Specimen C. It seems the capacity for this destroyed specimen can likely be recovered after repairing with CFRP composite sheets. However, its seismic performance was not as good as that of the repaired Specimen B. This repaired specimen was still not strong enough to resist such a large earthquake input.

Seismic Performance of Bridge Columns

Comparing the pseudodynamic test results shown in Figs. 11 and 12, it is very interesting to further explore why the as-built and the repaired Specimen B only experienced moderate damage under the ground acceleration of TCU075 with a peak ground acceleration of 0.8g while Specimen C experienced significant damage and ultimately failure under the ground acceleration of TCU102 with a peak ground acceleration of 0.7g. In order to gain insight into the difference in response between Specimens B and C, it is useful to calculate the Fourier response spectrum of the pseudodynamic displacement response time history for each pseudodynamic result and to construct the displacement response spectrum for the linear elastic SDOF systems. Even though the linear elastic displacement response spectrum cannot totally reflect the amplification effect in the displacement response for a highly inelastic reinforced concrete bridge column system, it is still indicative, because the variation of the structural frequency for the highly inelastic bridge column system can alternatively be considered as many linear elastic systems with different frequencies.

The four plots shown in Fig. 14 are obtained from the fast Fourier transforms of the numerical results of the top plots of Figs. 11 and 12. In Fig. 14, it can be found that the frequencies of the as-built and the repaired Specimen B were reduced during the pseudodynamic testing due to damage to the test specimen. In fact, the dominant frequencies for the as-built and repaired Specimen B tend to be about 2.5 Hz for a complete test and are much smaller than the initial structural frequency of 5.06 and 4.30 Hz for the as-built and repaired Specimen B. It is apparent that the frequency content of the repaired Specimen B is very similar to that of the as-built Specimen B. This comparison indicates that the seismic performance of the repaired Specimen B can be effectively recovered with CFRP composite sheets. On the other

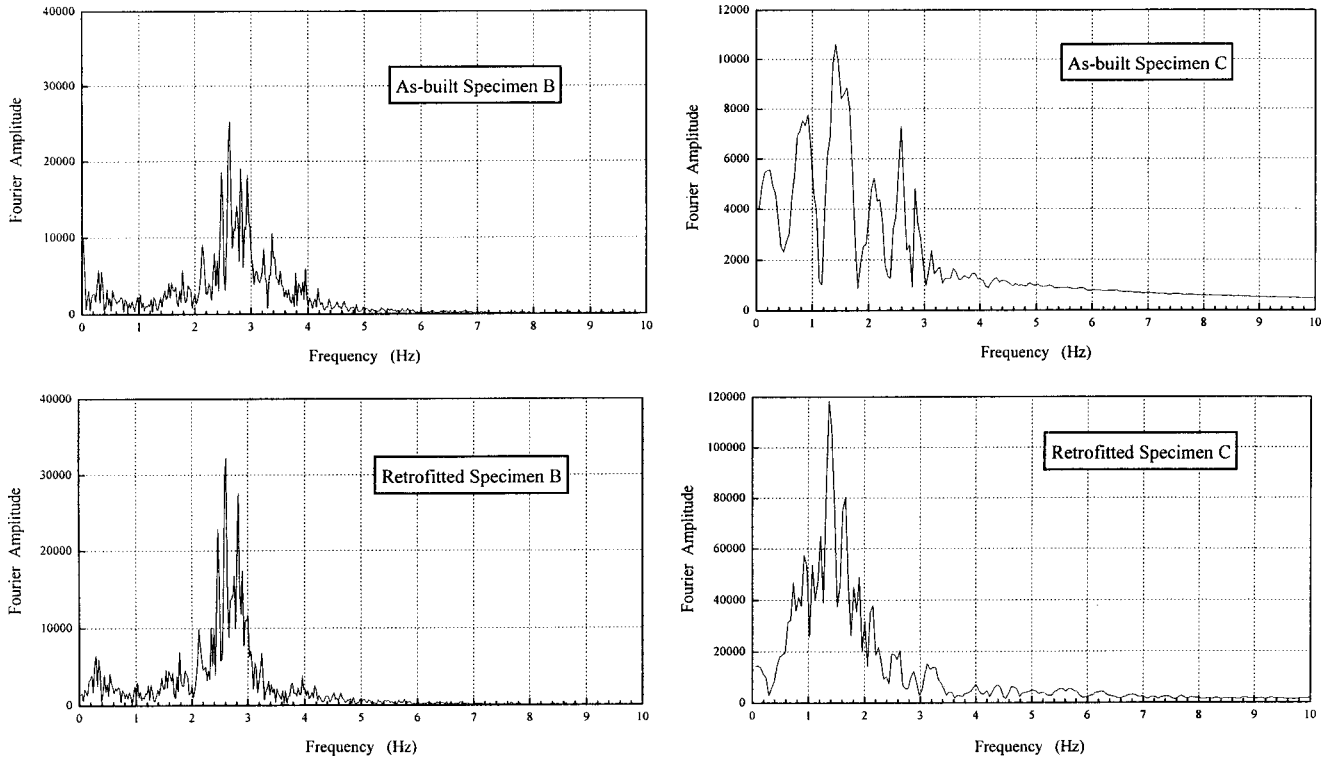

Fig. 14. Fourier amplitude of displacement response time history

hand, for Specimen C, the frequency content of the as-built column is quite different from that of the repaired column. It seems that there exist some explicit bands of dominant frequency over the range of 0–3 Hz for the as-built column. This dominant frequency might arise from the sudden spalling of concrete cover or sudden buckling of longitudinal bars, which will result in a large and rapid drop of lateral stiffness. As a result, some frequency content corresponding to the lateral stiffness drop is lost and the Fourier amplitudes for these specific frequencies are very small. Consequently, a significant valley is formed. Although the dominant frequency content for the repaired Specimen C spreads over the range of 0.5–2.5 Hz, there is no significant valley. This indicates that stiffness degradation occurs in a gradual manner. The gradual stiffness degradation is the result of the CFRP composite sheets, which provide a gradual increase in external confinement and avoid a sudden drop of lateral stiffness at least until the rupture of the CFRP composite sheets.

Displacement response spectra for linear elastic systems subjected to the ground acceleration of TCU075 with a peak ground acceleration of 0.8*g* and that of TCU102 with a peak ground acceleration of 0.7*g* are plotted in Fig. 15. It is apparent that, for a frequency in the range of 0–2 Hz, the spectral displacement is larger than the ultimate lateral displacement and consequently the specimen may have failed. Observing the top plot of Fig. 15, it is clear that Specimen B, either as-built or repaired, only experienced moderate damage, because the dominant frequencies are in the range of 2.5–3 Hz. On the other hand, failure of the as-built and repaired Specimen C is shown, as the dominant frequencies spread over the range of 0–3 Hz for the as-built Specimen C and 0.5–2.5 Hz for the repaired Specimen C.

In order to clarify why Specimen B could survive the pulse-like wave of TCU075 but Specimen C was destroyed by the pulse-like wave of TCU102, it is very important to consider the frequency right before the experience of the pulse-like wave. In fact, the stiffness for Specimen C is determined from the hysteretic curve in the time interval of $6.5 \leqslant t \leqslant 7$, because the peak

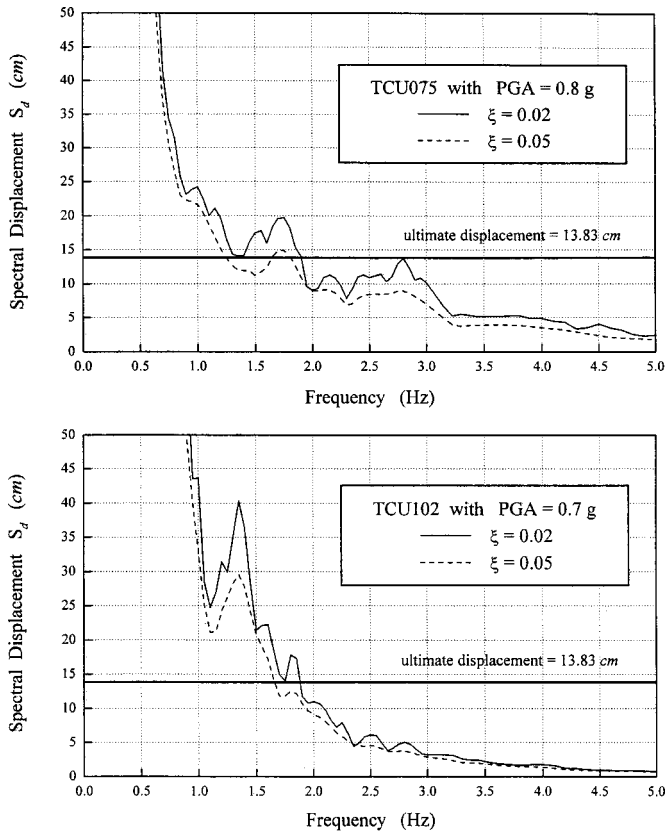

Fig. 15. Displacement response spectra to TCU075 and TCU102

Table 4. Estimated Structural Properties Right before Pulse-Like Wave

Property	As-built specimen		Repaired specimen	
	K_p (kN/cm)	f_p (Hz)	K_p (kN/cm)	f_p (Hz)
Specimen B	119.9	3.32	83.2	2.77
Specimen C	90.1	1.83	39.4	1.21

velocity occurs at $t=8.03$ s. Meanwhile, the hysteretic curve in the time interval of $15.5 \leqslant t \leqslant 16$ is used to determine the stiffness for Specimen C, because the peak velocity occurs at $t=16.78$ s. Results are summarized in Table 4. In addition, the corresponding natural frequencies are also included. In this table, K_p represents the stiffness right before the pulse-like wave and f_p denotes the corresponding structural frequency. In this table, the frequency for the as-built Specimen B is estimated to be 3.32 Hz right before the pulse-like wave. Thus, the spectral displacement is roughly estimated to be about 50 mm, which can be manifested from the top plot of Fig. 15. This displacement is far less than the ultimate lateral displacement; hence, this specimen can survive the pulse-like wave. A very similar phenomenon is also found for the repaired Specimen B. On the other hand, the frequency for the as-built Specimen C right before the pulse-like wave is found to be about 1.83 Hz. For this frequency, the spectral displacement is roughly about 175 mm and is greater than the ultimate lateral displacement; thus, the bridge column fails. Similar discussions can also be applied to the repaired Specimen C. A more accurate analysis of these pseudodynamic test results has been conducted (Li et al. 2003) using the Hilbert-Huang transform (Huang et al. 1998), because it can provide an instantaneous frequency response rather than the averaging frequency response provided by the fast Fourier transform.

Conclusions

It is a difficult task to accurately obtain the responses of reinforced concrete structures subjected to an earthquake ground motion using a numerical procedure, because it engenders the use of a load-displacement relationship. Hence, the pseudodynamic technique has been developed to overcome this difficulty by avoiding the use of a complicated load-displacement relation. In this study, seismic responses of as-built and repaired reinforced concrete bridge columns under near-fault ground motions were pseudodynamically obtained. CFRP composite sheets were used to repair the previously damaged test specimens. It is worth noting that the pseudodynamic response, such as the displacement response time history and the hysteretic response, can be considered as a reliable solution when an analytical model is proposed to mimic the load-displacement relation. In addition, some important results are strongly indicated by the cyclic loading test and pseudodynamic results. First, it is experimentally confirmed that the plastic moment estimated by the ACI 318 code is very reliable, because the flexural failure moment is almost the same as its predicted value. It seems that the seismic performance of the two damaged reinforced concrete bridge columns can be effectively recovered after repairing with CFRP composite sheets. Test results also show that a well-designed reinforced concrete bridge column, either as-built or repaired, may not be able to entirely develop full ductility, because a significant pulse-like wave may cause premature failure.

Acknowledgments

This study was supported by the National Science Council, Taipei 106, Taiwan, Republic of China, under Grant No. NSC-91-2711-3-319-200. All the experimental works were conducted at the National Center for Research on Earthquake Engineering (NCREE). Mr. His-Hsun Chen's assistance in handling the repair of specimens is appreciated. The first writer is also grateful for the technical support from NCREE, and especially Mr. Kung-Juin Wang and Chih-Hsiung Chou, who executed most of the experimental works.

References

American Association of State Highway and Transportation Officials (AASHTO). (1996). *Standard specifications for highway bridges*, 16th Ed., Washington, D.C.

Aschheim, M., and Moehle, J. P. (1992). ''Shear strength and deformability of reinforced concrete bridge columns subjected to inelastic cyclic displacement.'' *Rep. No. UCB/EERC-92/04*, Earthquake Engineering Research Center, Univ. of California at Berkeley, Berkeley, Calif.

California Department of Transportation (Caltrans). (1986). *Bridge design specifications manual*, Sacramento, Calif.

Chang, K. C., and Chang, H. F. (1999). ''Seismic retrofitting of existing reinforced concrete bridge columns using CFRP jacketing.'' *Rep. No. NCREE-99-030*, National Center for Research on Earthquake Engineering, Taipei, Taiwan.

Chang, S. Y. (1997). ''Improved numerical dissipation for explicit methods in pseudodynamic tests.'' *Earthquake Eng. Struct. Dyn.*, 26, 917–929.

Chang, S. Y. (2000). ''The γ-function pseudodynamic algorithm.'' *J. Earthquake Eng.*, 4(3), 303–320.

Chang, S. Y. (2001). ''Application of the momentum equations of motion to pseudodynamic testing.'' *Philos. Trans. R. Soc. London, Ser. A*, 359(1786), 1801–1827.

Chang, S. Y. (2002a). ''Explicit pseudodynamic algorithm with unconditional stability.'' *J. Eng. Mech.*, 128(9), 935–947.

Chang, S. Y. (2002b). ''An improved on-line dynamic testing method.'' *Eng. Struct.*, 24(5), 587–596.

Chang, S. Y. (2003). ''Nonlinear error propagation analysis for an explicit pseudodynamic algorithm.'' *J. Eng. Mech.*, 129(8), 841–850.

Chang, S. Y., Tsai, K. C., and Chen, K. C. (1998). ''Improved time integration for pseudodynamic tests.'' *Earthquake Eng. Struct. Dyn.*, 27, 711–730.

Huang, N. E., et al. (1998). ''The empirical mode decomposition and the Hilbert spectrum for nonlinear and non-stationary time series analysis.'' *Proc. R. Soc. London, Ser. A*, 454, 903–995.

Hwang, J. S., Hsieh, Y. M., Cheng, C. P., and Chou, C. H. (1999). ''Seismic retrofitting of existing reinforced concrete bridge columns using steel jacketing.'' *Rep. No. NCREE-99-016*, National Center for Research on Earthquake Engineering, Taipei, Taiwan.

Li, Y. F., and Chu, Y. C. (1999). ''A study of the FRP seismic retrofitting of circular piers (II).'' *Rep. No. NCREE-99-036*, National Center for Research on Earthquake Engineering, Taipei, Taiwan.

Li, Y. F., Chang, S. Y., Tzent, W. C., and Huang, K. (2003). ''The pseudodynamic test of bridge columns analyzed through Hilber-Huang transform.'' *Chin. J. Mech., Series A*, 19(3), 373–387.

Loh, C. H., Lee, Z. K., Wu, T. C., and Peng, S. Y. (2000). ''Ground motion characteristics of the Chi-Chi Earthquake of 21 September 1999.'' *Earthquake Eng. Struct. Dyn.*, 29, 867–897.

Newmark, N. M. (1959). ''A method of computation for structural dynamics.'' *J. Eng. Mech. Div.*, 85, 67–94.

Priestley, M. J. N., Seible, F., and Calvi, G. M. (1996). *Seismic design and retrofitting of bridges*, Wiley, New York.

Reinhorn, A. M., Simeonov, V., Mylonakis, G., and Reichman, Y. (1998). ''IDARC-Bridge: A computational platform for seismic damage as-

sessment of bridge structures.'' Rep. No. MCEER-98-0011, Multidisciplinary Center for Earthquake Engineering Research, State Univ. of New York at Buffalo, Buffalo, N.Y.

Shing, P. B., and Mahin, S. A. (1983). ''Experimental error propagation in pseudodynamic testing.'' *Rep. No. UCB/EERC-83/12*, Earthquake Engineering Research Center, Univ. of California at Berkeley, Berkeley, Calif.

Shing, P. B., and Mahin, S. A. (1984). ''Pseudodynamic method for seismic performance testing: Theory and implementation.'' *Rep. No. UCB/EERC-84/01*, Earthquake Engineering Research Center, Univ. of California, Berkeley, Calif.

Shing, P. B., and Mahin, S. A. (1987). ''Cumulative experimental errors in pseudodynamic tests.'' *Earthquake Eng. Struct. Dyn.*, 15, 409–424.

Shing, P. B., and Mahin, S. A. (1990). ''Experimental error effects in pseudodynamic testing.'' *J. Eng. Mech.*, 116(4), 805–821.

Taiwan Bridge Design Code. (1995). *Earthquake resistant design specifications for highway bridges*, Ministry of Communication and Transportation, Taipei, Taiwan.

Takanashi, K., Udagawa, K., Seki, M., Okada, T., and Tanaka, H. (1975). ''Nonlinear earthquake response analysis of structures by a computer-actuator on-line system.'' *Bulletin of the Earthquake Structure Resistance Center 8*, Institute of Industrial Science, Univ. of Tokyo, Tokyo.